공학석사 학위논문

냉각수 하단주입시의 Particle Bed Dryout 열유속

Dryout Heat Flux in Particle Beds with Forced Coolant Flow from Below

지도교수 방 광 현

2005 년 2 월

한국해양대학교 대학원

냉동공조공학과

김 종 명

Dryout Heat Flux in Particle Beds with Forced Coolant Flow from Below

by

Jong Myung Kim

Department of Refrigeration and Air-Conditioning Engineering Graduate School, Korea Maritime University

ABSTACT

The objective of the present study is to experimentally investigate the cooling of volumetrically heated particle beds and the enhancement of dryout heat flux in particle beds with coolant flow from below.

The experimental facility consists mainly of an induction heater (40 kW, 30 kHz), a quartz-tube test section containing 100 mm in diameter and 300 mm high particle bed, a water circulator and recovery condenser loop. The beads composing the particle bed are in uniform size and two sizes of beads were used; 3.2mm and 4.8 mm.

For the top-flooding case, the volumetric dryout heat rate was about 4 MW/m^3 in 4.8 mm particle and about 3 MW/m^3 in 3.2mm particle bed. For the bottom injection, the volumetric dryout heat rate was about 7.91 MW/m^3 in 4.8mm particle at the coolant injection mass flux of 1.5 kg/m^2s. In 3.2mm particle, the volumetric dryout heat rate was about 6.5 MW/m^3 at the coolant mass flux of 1.0 kg/m^2s. It shows the level of enhancement of dryout heat flux in particle beds with the forced coolant flow from below.

CONTENTS

NOMENCLATURE

A	surface area, m^2
A_{cross}	cross sectional area of debris bed, m^2
C_p	specific heat at constant pressure, J/kgK
$\bar{d}$	average diameter, mm
D	diameter, mm
G	mass flux, kg/m^2s
g	gravitational acceleration, m/s^2
H	bed height, mm
k	thermal conductivity, W/m-K
L	length, m
M	mass, kg
P	pressure, N/m^2
ΔP	pressure change, N/m^2
Q'''	volumetric power of the bed, W/m^3
$\dot{Q}$	heat transfer rate, kW
q''	heat flux, kW/m^2
T	temperature, ℃
u	superficial velocity

v	specific volume, m^3/kg
z	coordinate along the bed length, m

Greeks

Φ,	porosity
μ	dynamic viscosity, $N\text{-}s/m^2$
σ	surface tension, N/m
ρ	density, kg/m^3
κ	permeability
ν	kinematic viscosity, m^2/s

Subscripts

B	boiling
F	fluid
P	particle
S	solid
sat	saturation
sub	subcooling
Top	top of the bed
Bottom	bottom of the bed
Up	upward
Dn	downward

LIST OF TABLES

LIST OF FIGURES

CHAPTER 1

INTRODUCTION

1.1 Background

Transport and flow phenomena in porous media arise in many fields of science and engineering: agricultural, soil science, chemical and petroleum engineering.

A porous media has a complex structure and is affected by the flow, dispersion, and distribution. Many researchers have studied on the cooling of volumetrically heated particle beds. Particularly, is characterized as a particle bed of degraded nuclear reactor fuel, that structure is similar to porous media. The coolability of this heat generating particle bed is an important criterion in nuclear reactor safety. The degraded nuclear reactor fuel generates 2~4MW/m^3 of decay heat. But the cooling rate is limited by dryout heat rate. The dryout occurs due to the countercurrent flooding phenomena. At low power, the cooling of particle beds is achieved by thermal conduction enhanced by single-phase natural convection. At high power, boiling develops in the particle beds. Boiling is a very efficient cooling process. But the generation of high vapor flow rate prevents the occupied liquid region in particle beds and subsequently dryout occurs.

So, the bottom injection of coolant in the particle beds can increase dryout heat flux. The objective of this study is to experimentally investigate the enhancement of dryout heat flux in particle beds.

1.2 Research Objectives

The present study is to experimentally investigate the cooling of volumetrically heated particle beds with coolant flow from below. The objectives of this study are summarized as follows.

1. The definition, characterization, structure, flow and transfer of porous media are reviewed. Then, the past experimental studies on dryout heat flux in porous media are reviewed.
2. Experimental facility is designed and built to study the dryout heat flux in particle beds. It employs an induction heating method for volumetric heating.
3. The power distribution (spatial distribution) and temperature distribution are the major experimental measurements. It can provide an improved qualitative and quantitative understanding of dryout heat flux in particle bed.
4. The experimental results of dryout heat flux will be compared with existing experimental results, most of which are conducted with forced coolant flow from below in the bed.

CHAPTER 2

LITERATURE REVIEW

2.1 Introduction

Unlikely to the pipe flow, porosity is one of the important factors that affect fluid flow in particle beds. Porosity Φ is the volume fraction occupied by voids, the total void volume divided by the total volume occupied by the solid matrix and void volumes. The permeability, k, is defined by Darcy' law,

$$Q = \frac{k}{\mu} A \frac{\Delta P}{\ell} \tag{2.1}$$

where, Q is the volume flow rate, μ is the viscosity of fluid, A is the cross sectional area, $\triangle$P is the pressure drop. The permeability of a bed depends on porosity, particle shape and particle size distribution. The permeability is sometimes expressed in `darcys` where 1 darcy = $9.81\times10^{-13}\,m^2$.

Figure 2.1 shows the fluid flow in the structure of porous media. The dryout heat flux in particle beds will be discussed in this chapter with a focus on the effect of bed height, particle size, and coolant subcooling.

2.2 Characterization of Porous Media

The dryout heat flux in particle beds is affected by several parameters such as particle size, bed height, bed porosity, and pressure in bed, permeability, bed power and boundary conditions. The major controlling factors are known to be particle size, bed height, bottom cooling, and top subcooling.

2.2.1 Particle size

Experiments have shown that the dryout heat flux is changed by the particle size in particle beds. Generally, the dryout heat flux increases as the particle size increases. But the increasing trend is different according to the flow pattern (laminar and turbulent). For the laminar flow approximation as in the models of Dhir-Catton (1976), Hardee-Nilson (1977), Shires-Stevens (1980), and Jones (1980), it is shown that the dryout heat flux increases in the ratio of the square of the particle diameter. It is noted that all of these models were much fitted to the experimental data of the particle size range of 0.3 ~ 1.0 mm. In the case of the turbulent flow as in the Ostensen-Lipinski model (1981), it is shown that the dryout heat flux increases in the ratio of the square root of the particle diameter. But this model was much fitted to the cases of particle diameter range over 1 mm.

Considering the turbulent and capillary attraction, the Lipinski model (1980) is shown that the relationship between the dryout heat flux and the particle size can be expressed for the bed height H and the parameter λ_c which is given by

$$\lambda_c = \frac{\sigma(\varepsilon/\kappa)^{1/2}}{\sqrt{5}(\rho_f - \rho_g)g} \tag{2.2}$$

For small particle beds ($\ll$ 1 mm),

$$\lambda_c \langle H,\ q_d \approx d^2 \tag{2.3a}$$

$$\lambda_c \rangle H,\ q_d \approx d \tag{2.3b}$$

For large particle beds ($>$ 1 mm),

$$\lambda_c \langle H,\ q_d \approx \sqrt{d} \tag{2.4a}$$

$$\lambda_c \rangle H,\ q_d \neq d \tag{2.4b}$$

Figure 2.2 shows the change of dryout heat flux at each particle size.

2.2.2 Bed height

The height (or depth) of particle beds is not known to affect the dryout heat flux if it is regarded as so-called a deep bed. Figure 2.3 shows the dryout heat flux data of Westinghouse Co. Squarer (1981) reported that the bed was regarded as a deep bed if the bed height was more than 13 cm for the particle sizes of 0.5~0.6 mm. But as the particle size increases, the dryout heat flux increases.

Dhir (1984) proposed 10 cm of bed height for the limit of deep, above

which the dryout heat flux did not change. Hofmann (1984) observed that the limit was about 25 cm for 3 mm particle. But in the shallow bed, the dryout heat flux increases as the bed height decreases.

2.2.3 Coolant subcooling

Pool boiling and forced convective boiling have different trends due to the flow pattern. In the pool boiling case, the thicknesses of overlying coolant layer in particle beds has an influence on the dryout heat flux, but the effect of fluid subcooling on the dryout heat flux is low. According to the experimental results of Dhir-Catton, Squarer et al., and Barleon et al, the coolant subcooling does not affect the dryout heat flux.

In the forced convective boiling case, two flow directions are considered; the upward or the downward flow. Table 2.2 shows the experimental results of dryout heat flux with the forced convective flow. According to the experimental results, the dryout heat flux increases as the coolant mass velocity increases. In case the mass flux is large enough, the evaporation heat of coolant, $\varpi_f \left(h_{fg} + c_{pf}\Delta T_{sub}\right)$, may be considered.

2.3 Dryout Heat Flux in Porous Media

2.3.1 Pool boiling in porous media

In the past theoretical and experimental study, the dryout occurred because the coolant was not able to move into the lower particle bed. The particle beds can be submerged under the coolant pool. Dryout heat flux is very affected by the characterization of coolant and coolant properties. Many researchers have studied on the dryout heat flux in pool boiling. Table 1 summarizes the past work of pool boiling. It shows the range of particle size, bed height, particle material, heating method, and coolant type.

When the pool boiling occurs in particle beds, channels can be made in the top part of particle beds. This channel helps the vapor exit. But it only applies to a deep bed.

The dryout heat flux of pool boiling in particle beds generally increases as the particle size increases. Particle diameter range is over 4 mm. The dryout heat flux can be over the critical heat flux in the plate.

The dryout heat flux is higher in the shallow bed than the deep particle bed. The dryout heat flux of the deep particle beds (bed height is over 10 cm) is known independent of bed height. But In the shallow particle bed the dryout heat flux increases as the bed height decreases. If the particle bed height is sufficiently bigger than the particle diameter, the dryout heat flux is not changed by the particle diameter.

2.3.2 Forced convective boiling in porous media

Choudhary and E1-Wakil (1970) conducted a theoretical and experimental study on a volumetrically heated porous layer with the thermohydraulic characteristics of single-phase flow. They solved the coupled linear energy equations for the solid and gas phases using an implicit modified Crank-Nicholson method.

Hardee and Nilsion (1977) assumed that the low flows of reversed and upward vapor are separated individually. It is unlikely that the flow resistance controls the dryout heat. They suggested that vapor resistance control the dryout heat flux.

Dhir and Catton (1977) observed the dryout heat fluxes for inductively heated particle beds cooled from the top. This study dealt with two bed configurations, shallow and deep. Different mechanisms for the dryout in these beds were identified. It was concluded that the deep bed primarily dries out at a particular section in the lower region of the bed because gravity can no longer maintain the flow rate necessary to compensate for the evaporation rate. The evaporation rate is greater than the average downward superficial velocity of the coolant. Some semi-theoretical correlations were developed and validated based on the proposed hydrodynamic model.

Vasoliev and Mairov (1979, 1988) analyzed the heat transfer, pressure drop and stable characteristics of a volumetrically heated porous layer cooled with forced flow evaporation. Depending on the physical properties of the coolant, they divided the porous layer into three regions – subcooled, saturated two-phase mixture and superheated steam. For each region, they solved the energy equations with appropriating boundary and interfacial conditions to obtain temperature distribution in

the solid and the fluid. But the flow direction in this study is normal to the body force and the gravity acts in a direction parallel to the flow.

Shires and Stevens (1980) initially included the effect of capillary force between fluid and vapor. Jones (1980) provided the model of heating surface in deep layer on the base of fluid. The vapor is moving in opposite direction. The fluid flow is laminar.

Ostensen and Lipinski (1980, 1981) provided the result of dryout heat flux in deep layer on the basis of flooding. Lipinski introduced capillary force and surface force in turbulent flow. He developed the correlation of dryout heat flux for both upward and downward flow. Furthermore, he developed an abroad one-dimensional model of dryout heat flux.

Naik and Dhir (1982) experimentally investigated a volumetrically heated porous layer with coolant flowing through the layer. The purpose of this work was to obtain the data for the steady state temperature profile and pressure drop of an evaporating two-phase coolant flowing vertically. Based on the solution of the one-dimensional energy equations for the particles and the coolant with an assumption of no difference between the solid and liquid temperatures, a model for the temperature profile was developed. For the two–phase flow a separated flow model was based on the empirical relations obtained from the experiments. In this model, the void fraction was correlated as a function of the flow quality and mass flow rate. The model worked reasonably well for water-steam at atmospheric pressure. However this model was not good for the fluid mixtures with a higher vapor liquid volume ratio.

Hoffman (1984) investigated the result of experimental and analytical investigation on the dryout heat flux in inductively heated beds with both top and bottom injecting conditions. His model, which calculates the heat flux as a function of the saturation by solving the conservation equations

for momentum, mass and energy, gives a saturation distribution for dryout condition. But no satisfactory comparison was achieved with experimental data.

Generally the hydrodynamic models for predicting dryout are based on that the counter-current flooding controls dryout on porous media made up of large size particles.

Schulenberg and Muller (1984) performed experimental and analytical studies on hydrodynamic aspects of two-phase flow through porous media. The most of these studies were carried out for one-dimensional homogeneous porous layer. But what is encountered in actual practice is multidimensional. This may be composed of regions with widely varying permeability and heating conditions.

Tsai (1987) developed a dryout heat flux model for axi-symmetric porous layers with partial volumetric heating. His numerical solution was obtained by a finite difference scheme without the interfacial drag term. His solution through the use of the Lawrett function was included in capillary pressure. The solutions were applied to only for certain distribution of volumetric heating in the porous layers.

Tung and Dhir (1988) developed a hydrodynamic model to predict void fractions and pressure gradient for one-dimensional two-phase flow through porous media. The particle-gas drag, particle-liquid drag and liquid-gas interfacial drag were evaluated theoretically for the flow configurations associated with different flow regimes. The drag models were then employed in conjunction with force balances on the two phases to obtain the void fraction and pressure gradient as functions of liquid and gas superficial velocities.

The Lipinski model exemplifies the modeling approach of channeling of self-heated particle beds. It was assumed in this model that the vapor

pressure at the bottom of a channel is sufficient to offset the weight of the overlying particles plus liquid and the flow resistances in the channeled region are negligible.

Lipinski (1982,1984) suggested the idea of a sticking factor S_f, which means that the vapor pressure must be S_f times the overlying bed pressure at the bottom of a channel. However, it appears that a nondimensionalization of this sticking pressure leads straightforwardly to the sticking factor concept. The sticking factor model relies upon the analysis of the motion of particles caused by the upward displacement of a piston through the bed. Such a simulation is regarded as representative of the onset of channeling.

Stubos and Budhoin (1988, 1993) extended Lipinski's model by applying a force balance to a single bottom particles and the friction force. In details, they investigated the behavior of vapor channels traversing the upper part of a boiling, unconstricted, homogeneous particle bed. They suggested a theoretical model for the dryout heat flux in a channeled bed. They developed a multi-dimensional mathematical model for numerical analysis. They presented in assuming local thermal equilibrium (LTE) between the solid and liquid phases (thermally homogeneous medium). But this assumption may not be satisfactory for the step change problems during the early stages of the transport processes. There may be considerable differences between the temperatures of the flowing fluid and solid particles. This is also true even during the later stages of the transport processes in high-speed flows in which the fluid to solid interaction time may not be large enough to bring the temperatures of the fluid and solid phases close enough for LTE to be a reasonable assumption.

Sozen and Vafai (1990) were interested in non-thermal equilibrium

flow through a porous bed. They presented a general set of volume-averaged governing equations for non-thermal equilibrium condensing forced flow through a latent heat storage porous media. They carried out comprehensive numerical investigations of the phenomenon.

Kuznetsov (1994) made such an analysis based on solution of the full energy equations for incompressible fluid and solid phases without neglecting any terms in the equations by the perturbation technique. He showed that the temperature between the fluid and solid phases in a semi-infinite packed bed firms a wave localized in space. Later on, he investigated the thermal behavior of the three-dimensional porous bed during non-thermal equilibrium fluid flow through it.

2.4 Dryout Heat Flux Models

Dhir-Catton's model

When the deep beds are cooled by natural convection flow, the dryout is obtained (Figure 2.4). The assumptions in the model are:

1. The flow velocity is very low.
2. The steam vapor does not disturb the direction of coolant flow. The steam relative velocity is very low.
3. The cross sectional area occupied by vapor is very small.
4. The particle has a sphere shape and average weight in limited range.

In the relation of liquid and vapor, the density difference affects the coolant flow velocity in low region. The dryout heat flux is depending on the coolant flow velocity in low packed region. For the coolant flowing through low region, the momentum equation is

$$\frac{\mu f}{k} \cdot \frac{U}{(\bar{d})^2} = (\rho_f - \rho_g)g \qquad (2.5)$$

where k is permeability, $\bar{d}$ is the average diameter of particle.

In the cross section, the coolant superficial velocity u is

$$u = -\frac{\kappa}{\mu_f}(\rho_f - \rho_g)g(\bar{d})^2 \qquad (2.6)$$

Appling porosity ε and permeability k

$$\kappa \sim \frac{\varepsilon^3}{(1-\varepsilon)^2} \tag{2.7}$$

$$u = c_1 \frac{\varepsilon^3}{(1-\varepsilon)^2} \frac{(\bar{d})^2(\rho_f - \rho_g)g}{\mu_f} \tag{2.8}$$

Here c_1 is an experimental value.

According to energy momentum equilibrium,

$$q = \rho_f h_{fg} u \tag{2.9}$$

or

$$q = c_1 \frac{\varepsilon^3(\bar{d})^2}{(1-\varepsilon)^2} \frac{\rho_f h_{fg}(\rho_f - \rho_g)g}{\mu_f} \tag{2.10}$$

The authors experimentally investigated the cooling in inductively heated particle beds. Water, methanol, and acetone were used as coolants. Based on the experimental result, they proposed $c_1=10^{-4}$. Gabor and Sowa obtained the dryout heat flux data in the low heated region and proposed $c_1=10^5$ for the equation (2.10).

Hardee-Nilson's model

In the two-phase region, water has a downward direction and the vapor has an upward direction. Upward fluid turns to the vapor at the top region. The energy equation becomes,

$$\gamma\rho_f u_f c_f (T_B - T_C) + (1-\gamma)u_g\rho_g h_{fg} = QH \tag{2.11}$$

where γ is a volume flow rate of fluid and Q is heat generation rate per volume.

The momentum equation is,

$$\gamma \rho_f u_f c_f = (1 - \gamma) \rho_g u_g \tag{2.12}$$

In the Darcy's law, the downward fluid velocity is,

$$u_f = \frac{k}{\mu_f} \left(\rho_f - \frac{dP}{dz} \right) \tag{2.13}$$

and the upward fluid velocity is,

$$u_g = \frac{k}{\mu_g} \left(\frac{dP}{dz} - \rho_g g \right) \tag{2.14}$$

If the vapor density is very small,

$$u_g = \frac{k}{\mu_g} \left(\frac{dP}{dz} \right) \tag{2.15}$$

Combining equations (2.11) and (2.12), $\rho_g g$ is removed.

$$\gamma \rho_f u_f c_f (T_B - T_C) + h_{fg} = QH \tag{2.16}$$

In equations (2.13) and (2.15), $\frac{dP}{dz}$ is removed.

$$\frac{u_f \mu_f}{k} = \rho_f g - \frac{u_g \mu_g}{k} \tag{2.17}$$

$$u_g = \frac{\gamma}{1-\gamma} \frac{\rho_f u_f}{\rho_g} \tag{2.18}$$

To the equation (2.17), applying the continuity equation,

$$\rho_f u_f \left(\nu_f + \frac{\gamma}{1-\gamma} \nu_g \right) = \rho_f g k \tag{2.19}$$

where ν is kinetic viscosity coefficient.

From the equations (2.16) and (2.19),

$$Q = \frac{\gamma \left[c_f (T_B - T_C) + h_{fg} \right] g k \rho_f}{H \left(\nu_f + \frac{\gamma}{1-\gamma} \nu_g \right)} \tag{2.20}$$

$$\frac{d}{dr} \left[\frac{QH}{c_f (T_B - T_C) + h_{fg}} \right] = 0 \tag{2.21}$$

and these lead to,

$$\frac{1-\gamma}{\gamma} = \left(\frac{\nu_g}{\nu_f} \right)^{1/2} \tag{2.22}$$

$$\gamma = \frac{1}{\left(\frac{\nu_g}{\nu_f}\right)^{1/2} + 1} \tag{2.23}$$

$$Q_d = \frac{gk\rho_f h_{fg}}{H_{\nu_g}} \frac{\left[1 + c_f (T_{boing} - T_c) / h_{fg}\right]}{\left[1 - (\nu_f / \nu_g)^{1/2}\right]^2} \tag{2.24}$$

Using the Kozeny relation equation,

$$k = \frac{\bar{d}^2}{180} \frac{\varepsilon^3}{(1 - \varepsilon)^2} \tag{2.25}$$

After equation (2.15) is substituted, dryout heat flux $q_d(Q_d H)$ in the top region is written as,

$$q_d(Q_d H) = \frac{\bar{d}^2}{180} \frac{\varepsilon^3}{(1 - \varepsilon)^2} \frac{g\rho_f h_{fg}}{\nu_g} \left[1 + \left(\frac{\nu_f}{\nu_g}\right)^{1/2}\right]^{-2} \tag{2.26}$$

Shires-Stevens model

They considered that the dryout heat flux was affected by the capillary pressure in particle bed.

$$\Delta P = \frac{6\sigma}{c'} \frac{(1 - \varepsilon)}{\varepsilon} \frac{1}{d} \tag{2.27}$$

where c' is an integer number.

Then the dryout heat flux is,

$$q_d = c_2 \frac{d^2}{180} \frac{\varepsilon^3}{(1-\varepsilon)^2} \frac{g(\rho_f - \rho_g)h_{fg}}{\nu_g} \times \left[1 + \frac{4.3\sigma(1-\varepsilon)}{g(\rho_f - \rho_g)gfH}\right] \quad (2.28)$$

Jones et al.

They proposed a dryout heat flux model for heated particle beds with coolant from below. The assumptions were

1. Vapor and liquid flows have the opposite direction passing through the particle beds.
2. The particle has sphere shape and uniform in size.
3. All vaporization occurs in the low region.
4. The flow is laminar.
5. The shape of the liquid and vapor boundary surface is similar to the shape of the liquid and solid boundary surface.
6. The peripheral length is proportioned to the square root of flow surface.

Bird obtained the dryout heat flux on the basis of Blake-Kozency equation.

$$q_d = \frac{\bar{d}^2}{150} \frac{\varepsilon^3}{(1-\varepsilon)^2} \frac{g(\rho_f - \rho_g)h_{fg}}{\nu_g} \times \left[\frac{1}{\alpha^3(1-\alpha)} + \frac{\nu_f}{\nu_g} \frac{1}{(1-\alpha)^3} \right]^{-1} \quad (2.29)$$

Ostensen-Lipinski model

They obtained the dryout correlation on the basis of flooding criterion (phenomenon) in particle beds. The particle size was over 1 mm and the flow was assumed turbulent.

From the experimental measurements,

$$u_f^{*1/2} + u_g^{*1/2} = 0.775 \quad (2.30)$$

$$u_g^* = u_g \left(\frac{\rho_g}{gD\rho_f \varepsilon^2} \right)^{1/2} \quad (2.31)$$

$$u_f^* = u_g \Big/ (gD\varepsilon^2)^{1/2^{1/2}} \quad (2.32)$$

u_g = upward vapor velocity

u_f = downward liquid velocity

D = the ratio of fluid volume over the particle surface area.

The surface force is very small so it was ignored. The particle sizes are

bigger than the flooding criterion.

The continuity equation is,

$$\rho_f u_f = \rho_g u_g \tag{2.32}$$

In the flooding criterion, vapor velocity $u_{g,f}$ is given

$$u_{g,f} = \frac{0.601(gD\varepsilon^2 \rho_f / \rho_g)^{1/2}}{\left[1 + (\rho_g / \rho_f)^{1/4}\right]^2} \tag{2.33}$$

The vapor velocity is very high in the top region. Dryout heat flux is

$$q_d = \rho_g h_{fg} u_{g,f} \tag{2.34}$$

$$D = \frac{\varepsilon}{(1 - \varepsilon)S} \tag{2.35}$$

D is the ratio of the particle surface over the particle volume.

Therefore,

$$q_d = \frac{0.601 h_{fg} \left[\rho_f \rho_g g\varepsilon / S(1 - \varepsilon)\right]^{1/2}}{\left[1 + (\rho_g / \rho_f)^{1/4}\right]^2} \tag{2.36}$$

If the particle layer consists of uniform shape, $S = \frac{6}{d}$

$$q_d = \frac{0.245 h_{fg} \left[\rho_f \rho_g g d \varepsilon^3 / (1 - \varepsilon)\right]^{1/2}}{\left[1 + (\rho_g / \rho_f)^{1/4}\right]^2} \quad (2.37)$$

Ostensen-Lipinski model shows that the dryout heat flux is proportional to the square root of particle diameter. Equation (2.37) shows a good agreement with the experimental results for large size particles.

Standard model of Lipinski

This model is an expanded of the Hardee-Nilson model. It included the turbulent flow and the effect of capillary pressure proposed by Shires-Stevens. The correlation also included the upward and downward boiling. Two-phase fluids are passing through particle beds and the two fluids have an opposite direction. The conservation equations are,

$$\frac{\rho_g}{\eta \eta_g} u_g^2 + \frac{\mu_g}{k k_g} u_g - \frac{\Delta P_g}{H} + \rho_g g = 0 \quad (2.38a)$$

$$- \frac{\rho_f}{\eta \eta_f} u_f^2 - \frac{\mu_f}{k k_f} u_f - \frac{\Delta P_f}{H} + \rho_g g = 0 \quad (2.38b)$$

$$\rho_g u_g h_{fg} = QH \quad (2.39)$$

$$\rho_g u_g - \rho_f u_f = 0 \quad (2.40)$$

$$\Delta P_g - \Delta P_f = \sigma \left(\frac{\varepsilon}{5k}\right)^{1/2} \quad (2.41)$$

ΔP = pressure drop through the debris bed

Q = volumetric heating rate

K= permeability

k_f, k_g = nonpermeability

η, η_g, η_f = turbulent factor

From the Kozeny-Carman correlation,

$$k = \frac{\bar{d}^2}{180} \frac{\varepsilon^3}{(1 - \varepsilon)^2} \tag{2.42}$$

$$\eta = \frac{d}{1.75} \frac{\varepsilon^3}{1 - \varepsilon} \tag{2.43}$$

Appling to the experimental nonpermeability,

$$k_g = 1 - 1.11\gamma \tag{2.44a}$$

$$k_f = \gamma^3 \tag{2.44b}$$

γ is a fluid volume rate. The turbulent factors are,

$$\eta_g = (1 - \gamma)^3 \tag{2.45a}$$

$$\eta_f = \gamma^3 \tag{2.45b}$$

In the heated particle beds,

$$q = \rho_g h_{fg} \left[\left(u_l^2 + u_t^2 \right)^{1/2} - u_l \right] \tag{2.46}$$

Here,

$$u_l = \frac{\eta}{2k\rho_g} \left(\frac{\nu_g}{k_g} + \frac{\nu_f}{k_f} \right) \Bigg/ \left(\frac{1}{\rho_g \eta_g} + \frac{1}{\rho_f \eta_f} \right) \tag{2.47}$$

$$u_t = \left[\frac{\eta(\rho_g - \rho_f)g}{\rho_g^{\,2}} (1 + \lambda_c / H) \Bigg/ \frac{1}{\rho_g \eta_g} + \frac{1}{\rho_f \eta_f} \right]^{1/2} \tag{2.48}$$

$$\lambda_c = \frac{\sigma(\varepsilon/k)^{1/2}}{\sqrt{5}(\rho_g - \rho_f)g} \tag{2.49}$$

In the bed of small particles ($d \langle\langle 1mm$),

$$q_d = q_0 (1 + \lambda_c / H) \tag{2.50}$$

$$q_0 = g k h_{fg} (\rho_g - \rho_f) \left[\frac{\nu_g}{1 - 1.11} + \frac{\nu_f}{\gamma^3} \right]^{-1} \tag{2.51}$$

$$\gamma = \left[0.833\, \nu_f / \nu_g + (2.07\, \nu_f / \nu_g)^{1/2} \right]^{1/2} - (0.833\, \nu_f / \nu_g)^{1/2} \tag{2.52}$$

$H \rangle \lambda_c$, q_d changes proportional to the square of particle diameter.

$H \langle \lambda_c$, q_d changes as a function of bed depth and particle diameter.

For the large particle bed ($d \rangle 1mm$),

$$q_d = \frac{h_{fg}\left[\rho_g(\rho_f - \rho_g)g\eta(1 + \lambda_c/H)\right]^{1/2}}{\left[1 + (\rho_g/\rho_f)^{1/4}\right]^2} \qquad (2.53)$$

$H \rangle \lambda_c$, q_d changes proportional to the square of particle diameter.

$H \langle \lambda_c$, q_d is independent of particle diameter.

Figure 2.6 shows the comparison of dryout heat flux predictions of each model for the particle bed, 100 mm high, atmosphere pressure, and porosity $\varepsilon = 0.4$. The Dhir-Catton and Hardee-Nilson models are good for the small particle size, Shires-stevens model for the medium particle size. The prediction of Ostensen-Lipinski model is close to the Lipinski's for larger particle size.

The upward and downward boiling,

$$q_{up} = \frac{q_0}{2}\left\{\frac{2\lambda_c}{H} + \left[\left(\frac{2\lambda_c}{H}\right)^2\right]^{1/2} + 1 + 1\right\} \qquad (2.54)$$

$$q_{down} = \frac{q_0}{2}\left\{\frac{2\lambda_c}{H} + \left[\left(\frac{2\lambda_c}{H}\right)^2 + 1\right]^{1/2} - 1\right\} \qquad (2.55)$$

The capillary force drags the liquid from the bottom to the top. The vapor is down to the bottom. This phenomenon is downward boiling. The number $\frac{\lambda_c}{H}$ of an equation that capillary force term is negative will give the standard form of dryout heat flux in the downward boiling range.

One-dimensional model of Lipinski

This model included the effect of laminar, turbulent, two-phase flow, capillary pressure, and channel in particle beds. Also, it can be applied to the cases that the bed bottom was either heating or cooling. Figure 2.7 shows the liquid and vapor flow fields in a uniform-size particle bed. If the particle size is uniform and the low plate is insulated, the energy and mass equations in the packed region of particle beds are,

$$\frac{d}{dz}\left(\rho_g,\ u_g,\ h_{fg}\right) = Q \qquad (2.56a)$$

$$\frac{d}{dz}\left(\rho_g u_g + \rho_f u_f\right) = 0 \qquad (2.56b)$$

Q is the volumetric heat generation rate. In closed plate,

$$\rho_g u_g h_{fg} = \int_0^x Q dz = q \qquad (2.57)$$

And

$$\rho_g u_g + \rho_f u_f = \omega \tag{2.58}$$

Here, q(=Qz) is the dryout heat flux at the elevation z and ω is the mass flux of coolant injection from below. From Ergun equation of pressure drop through the particle beds, momentum conservation equation is

$$\frac{1.75(1-\varepsilon)\rho_g u_g |u_g|}{\eta_g \varepsilon^3 d} + \frac{150(1-\varepsilon)^2 \mu_f u_f}{k_g \varepsilon^3 d^2} + \frac{dP_g}{dz} + \rho_g g = 0 \tag{2.59a}$$

$$\frac{1.75(1-\varepsilon)\rho_f u_f |u_f|}{\eta_f \varepsilon^3 d} + \frac{150(1-\varepsilon)^2 \mu_f u_f}{k_f \varepsilon^3 d^2} + \frac{dP_f}{dz} + \rho_f g = 0 \tag{2.59b}$$

Here, k_f, k_g is relative possibility of liquid and vapor and η_f , $\eta_g$is the turbulent values of k_f, k_g. Brooks and Corey proposed,

$$k_g = (1-s)^3 \tag{2.60a}$$

$$k_f = s^3 \tag{2.60b}$$

S is the effective saturation of particle layer.

$$s = \frac{s_t - s_r}{1 - s_r} \tag{2.61}$$

s_t is true saturation

s_r is residual saturation

Brown suggests

$$s_r = \frac{1}{22}\left[\frac{(1-\varepsilon)^2 \sigma \cos\theta}{d^2 \varepsilon^3 \rho_{fg}}\right]^{0.264} \tag{2.62}$$

Reed suggests the relative permeability in turbulent fluid flow,

$$\eta_g = (1-s)^5 \tag{2.63a}$$

$$\eta_f = s^5 \tag{2.63b}$$

For the difference between P_g and P_f, and the Leverett function J,

$$P_g - P_f = \frac{\sqrt{150}\,\sigma (1-\varepsilon) \cos\theta J}{\varepsilon d} \tag{2.64}$$

$$J = \frac{(s^{-1}-1)P_L}{\sqrt{5}} \tag{2.65}$$

P_L =0.175 (experience value)

Combining the equations (2.57), (2.60), (2.63), (2.64) and (2.65),

$$\frac{\sqrt{150}\sigma \cos\theta(1-\varepsilon)}{\varepsilon d}\frac{dJ}{ds}\frac{ds}{dz} + \sqrt{150}\sigma \cos\theta J \frac{d}{dz}\left(\frac{1-\varepsilon}{\varepsilon d}\right) - (\rho_f - \rho_g)g + \frac{0.175(1-\varepsilon)q^2}{h_{fg}^2\varepsilon^3 d}\left[\frac{1}{\rho_g(1-s)^5} \pm \frac{1}{\rho_f s^5}\right] + \frac{150(1-\varepsilon)^2 q}{h_{fg}\varepsilon^3 d^2}\left[\frac{\mu_g}{\rho_g(1-s)^3} + \frac{\mu_f}{\rho_f s^3}\right] + \frac{(1-\varepsilon)\omega}{\rho_f\varepsilon^3 d} \times \left[\pm \frac{1.75\omega}{s^5} \mp \frac{3.5q}{s^5 h_{fg}} - \frac{150(1-\varepsilon)\mu_f}{s^3 d}\right] = 0 \quad (2.66)$$

$q>\omega h_{fg}$ is applied to the upper sign.

$q<\omega h_{fg}$ is applied to the lower sign.

Table 2.1 Past experimental studies on dryout heat flux

Author	Particle Size (mm)	Particle Materials	Bed Diameter Height (mm)	Coolant Materials
Dhir-Catton	0.295~ 0.787	Steel, Lead	47 190~890	Water Acetone Methanol
Hardee-Nilson	?	Silica sand	50, 120 360	Nacl/Water
Shires-Stevens	0.68 1.2 2.0	Steel	30~195	Water
Jones et al	0.35~ 1.095	Steel Lead Cu	480 80~300	Water Acetone Methanol Isopropanol
Barleon-Werle	2~15.88	Stainless Steel	80 80	Water Freon-113
Squarer et al	0.55~11.11	Stainless Steel	102 127~305	Water
Theofanous Et al	1~20	Al Gravel	100	Water
Hofmann	3	Stainless Steel	606 50	Water
Tsai et al	1.588 3.175 4.763	Steel	690 80~150	Freon-113

Table 2.2 Dryout heat flux data of some selected past work

Authors	Particle Size mm	Bed Height m	Mass Flux kg/m^2s	Vol. Dryout Heat MW/m^3
Barleon et al. (1981)	0.06-16	< 0.4	0	0.7~6
Tsai & Catton (1983)	0.6-4.8	< 0.15	0-0.56	3~4
Hu & Theofanous (1991)	7-9	1.02	0	0.6~1
Cha et al. (1986)	1.5-5	0.11	0-3.5	9~26
Atkhen & Berthoud (2003)	2-7.2	0.5	?	1.6~5.4

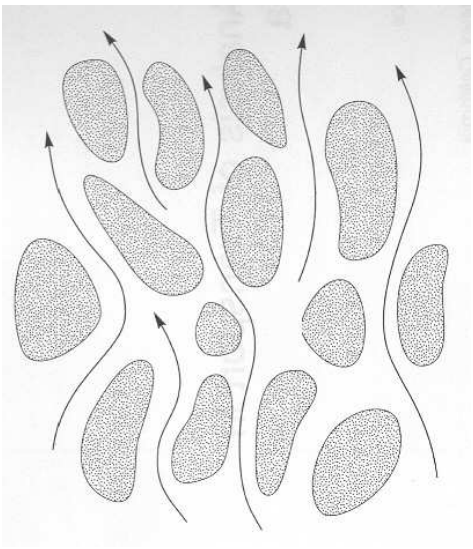

Figure 2.1 Fluid flow in the structure of particle bed

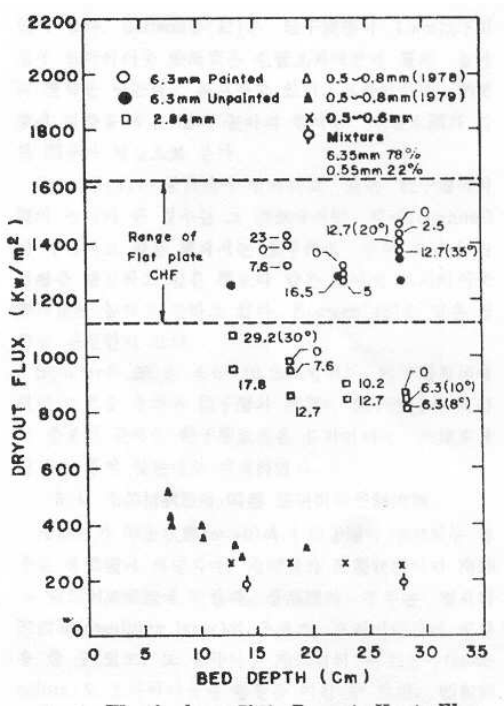

Figure 2.2 Effect of bed depth on dryout heat flux

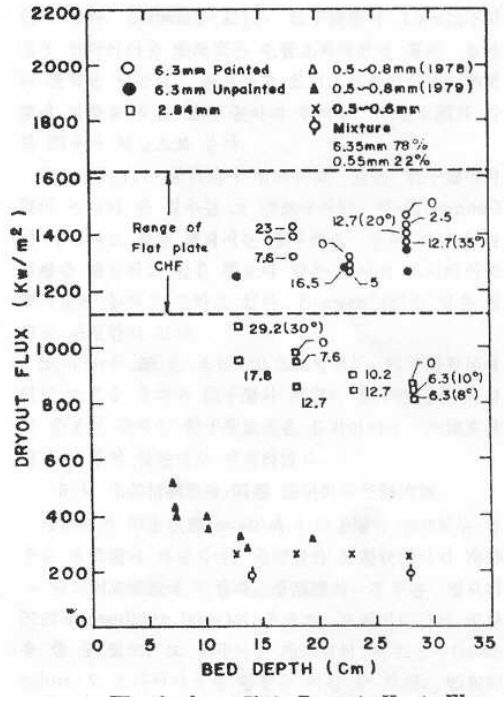

Figure 2.3 Dryout heat flux of Westinghouse co.

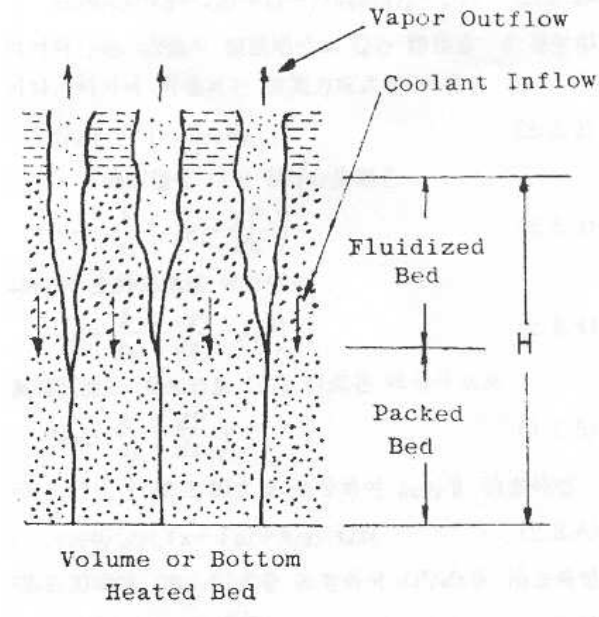

Figure 2.4 Model of the Dhir-Catton

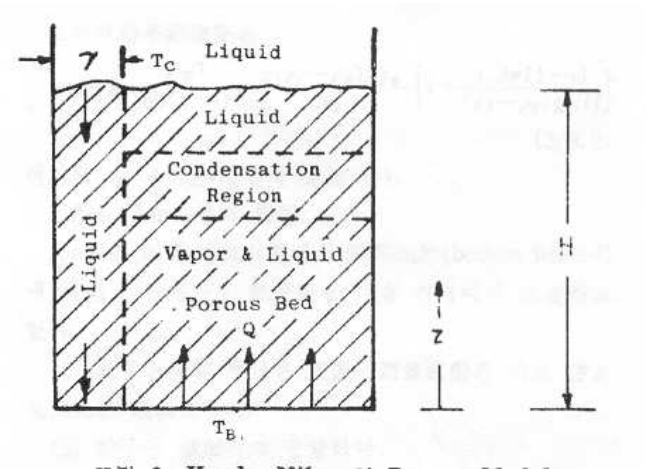

Figure 2.5 Model of the Hardee-Nilson

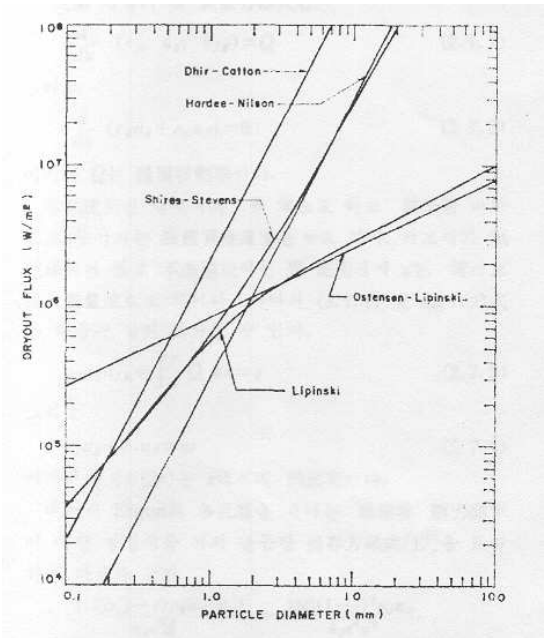

Figure 2.6 Comparison of dryout heat flux models

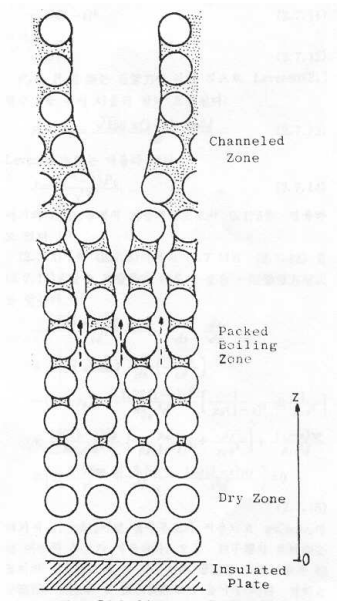

Figure 2.7 One-dimensional dryout model of Lipinski

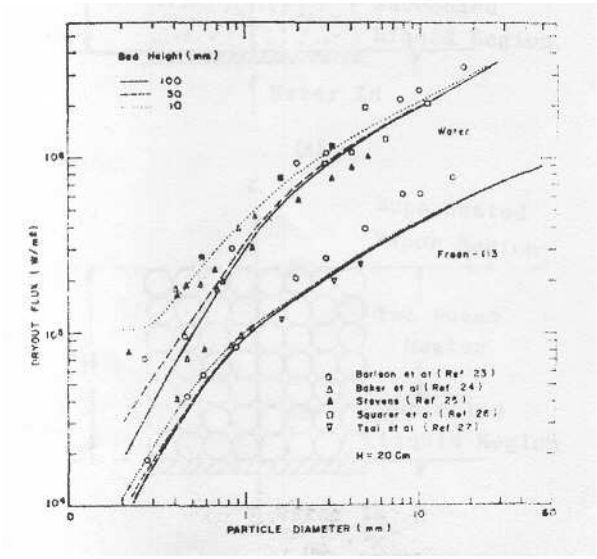

Figure 2.8 Comparison of Lipinski 1-dimensional model and experimental data

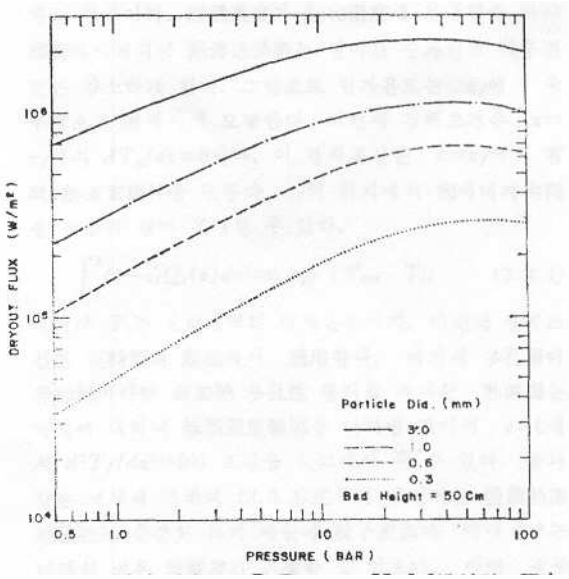

Figure 2.9 Pressure effect of Lipinski 1-dimensional model

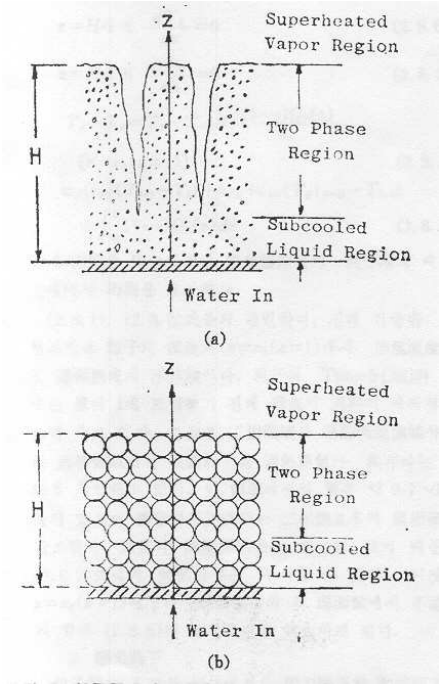

Figure 2.10 Forced convective boiling in particle bed

(a: large size particle, b: small size particle)

CHAPTER 3

EXPERIMENTAL SETUP

3.1 Experimental Facility

An experimental setup for long-term coolability in volumetrically heated particle beds with coolant injected from below was constructed. The experimental apparatus mainly consists of an induction heater system, a quartz tube test section containing particle bed, a condenser, and a water circulator. A schematic diagram of the apparatus is shown in Fig. 3. 1.

3.1.1 Test particle bed and induction heater

The particle beds are composed of steel particles in a quartz tube. The shape is spherical and the steel particle sizes are 3.2mm and 4.8mm. The tube is made of quartz and the height is 300mm and the inner diameter is 100mm.

The test section is a double-walled quartz tube. It was fabricated with 3 mm thick quartz tube and it can contain up to 300 mm high particle bed. Uniform-size steel beads were charged into the test tube to build a particle bed. The lower part of the test section was filled with glass balls to separate the steel particle bed and the joining flange and also to distribute the water coolant uniformly over the cross section of the

bottom of the particle bed when the coolant was injected from below. The particle beds were inductively heated in a double-wall glass vessel, which is open at the top (atmospheric pressure). The double-wall sidewall was intended to minimize heat loss. The gap was open to the atmosphere.

Water was the coolant for particle beds with forced flow from below. The heating up rate in the bed filled with stagnant water measured at different spatial positions was used for the power density distribution within the bed. This good homogeneity of power was achieved by electrically insulating the particles mutually. The insulation was offered by oxide surface layer. The oxide coating was made naturally, that is, it occurred during the preliminary boiling tests. As far as the beads are oxidized, the magnetic field penetrates more and more within the bed. The heat produced in the bed is removed either only from the top or by the injected water from below.

Twenty three chromel-alummel(K-type) thermocouples (sheathed, 1.6 mm diameter) were located at different positions within the bed (Fig. 3. 3). The radial distribution of the thermocouples is also shown in the Fig. 3. 4. Thermocouples were located in five vertical levels inside the bed (Fig. 3. 3). The porosity Φ has been determined for 100 mm diameter and 300 mm high bed. The measured porosity for the 4.8mm particles was $\Phi = 0.38$ and 0.37 for the 3.2mm particles (Table 3. 1).

Water was flooded at the top of the bed in the atmospheric pressure or injected at the bottom of the bed. The generated vapor is passed to a condenser, and the condensate flow rate and temperature were measured. The collected liquid was redirected to the bed at a controlled temperature close to T= 95℃.

The induction heater system consists of power supply and control unit (40 kW, 30 kHz), an induction coil and a cooling unit (Fig. 3. 2). The brine coolant of the cooling unit is also directed to the condenser unit to condense the steam produced in the test section.

3.1.2 Instrumentations

The steam condenser is a shell-and-tube type heat exchanger and the coolant of the induction heater unit is also used for the condenser (Fig. 3. 5). The condenser cooling surface area is 1.31m^2.

The condensate liquid flow rate is measured and the condensate liquid water is returned to the water circulator (Fig. 3. 6). The water circulator temperature range is from –30 to 150℃.

The circulator has a 15 lpm at 0`(0m) of pumping capacity and the reservoir volume is 13 liters. The water circulator supplies water coolant to the test section at a predetermined temperature either to the top of the test section (top-flooding tests) or from below of the test section (bottom injection tests). The water coolant flow rate is controlled by use of a constant-speed pump and a needle valve.

The measurements were made for coolant temperatures inside the bed at various radial and axial locations, and for the flow rates of water coolant supply and the condensate liquid flow.

A coriolis-type mass flow meter (Fig. 3. 7) was used to measure the coolant injection rate and a rotameter (Fig. 3. 8) was used for condensate liquid flow rate measurement. The thermocouples and flow meter signals were processed, monitored, and recorded in a PC-based data acquisition system (Labview, Fig. 3. 9). The data acquisition system was made by National Instruments Company (Fig. 3. 10).

3.2 Experimental Procedure

For the first test series, a mono-disperse bed with pre-oxidized 4.8mm spheres (height 300mm) under atmospheric conditions was used. The measured bed porosity 0.38 was depending of the level of rust.

For the second test series, pre-oxidized 3.2mm particle spheres (height 300mm) under atmospheric conditions were used. The bed porosity was 0.37 in single-phase flow experiments. Other test conditions were the same.

This setup allows pool boiling experiments with no additional water injection (counter-current-flow, with condensate from the condenser fed to the top of the bed), as well as experiments with water injection from the bottom (co-current-flow)

The tests were conducted according to the following procedure:

(1) Turn on the pump and heat the coolant in the circulator to the nearly 95 degrees to be injected to the particle bed.

(2) Adjust the valves for a desired coolant flow rate while the induction heater turned on for warming-up.

(3) The induction heater power button turned on and the power is increased in steps.

(4) At each power level, the test is running for 15~30minutes of time to allow any delayed dryout of the bed.

(5) The dryout of the bed is observed visually by monitoring the sharp rise in the temperature of one or more of the thermocouples in the bed.

(6) The power is turned off as soon as dryout is observed. The bed is cooled by the natural convection for about 20 minutes.

(7) Repeat at least once more under the same test conditions.

(8) For different set of test conditions, repeat step1 through step 6.

3.3 Data Reduction

3.3.1 Temperature measurement

Twenty three chromel-alummel(K-type) thermocouples (sheathed, 1.6 mm diameter) were inserted inside the bed at five axial locations, 50 mm apart, as shown in Fig. 3. 2. The radial distribution of the thermocouples is also shown in the figure. Several thermocouples are soldered in the center of a bead. A set of 23 thermocouples located in the median plane of particle beds. The thermocouples are installed when the bed is filled with the beads, so that the main vertical flow is not disturbed. They are located where dryout areas are expected; there are divide into each level at 50mm intervals (Fig. 3. 3).

3.3.2 Heat spatial distribution

Expected to homogeneous beds and homogeneous volumetric heating. But a nonhomogeneous bed and nonuniform volumetric heating may characterize a realistic particle beds.

In our case, and because of skin effects, using an induction coil leads to a heterogeneous power distribution within the bed, Especially in the middle of bed, the density of the volumetric heat source can be ~10% higher than the average value, whereas in the top and bottom of the bed, the local heat source can be 10% lower. As a consequence, I am averaging the values of the density in the volumetric heat source.

3.3.3 Calculation of volumetric power density

As the uniformity of power distribution identical in the particle bed, I decided to the increment of each located thermocouples region.

$$q''' = \frac{Q}{V} = \left(\frac{m}{V}\right)\bar{c}_p \frac{dT}{dt} = \bar{\rho}\ \bar{c}_p \frac{dT}{dt} \quad (1)$$

Here, $\bar{\rho}, \bar{c}_p$ have including values of steel sphere and around water.

Naming Porosity ϕ,

$$\bar{\rho} = \frac{m}{V} = \rho_{steel}(1 - \phi) + \rho_{water}\phi \quad (2)$$

$$\bar{c}_p = \frac{1}{\bar{\rho}}\left[\rho_{steel}(1 - \phi)c_{p,steel} + \rho_{water}\phi c_{p,water}\right] \quad (3)$$

To this particle bed is uniform, $\bar{\rho}, \bar{c}_p$ are equal.

Because of the comparison of measuring temperature change, I decided an identical to the power density.

In order to measure the volumetric power density in the bed induction heating, liquid coolant was filled up to the top of the bed and induction power was applied at a predetermined level. The liquid temperature was allowed to rise to the boiling temperature. Figure 4. 2 is shown the rising temperature.

The twenty-two thermocouple signals gave sensible heating of liquid and these values were converted to power density distribution. In the

upper part of the bed, observing the nonlinear rise of temperature. It caused the natural circulation of coolant in the bed. Although the center of the bed showed higher power and the top and the bottom parts of the bed were lower, the power density was uniform within 10%. The average power density at different power level of the induction unit is shown in Fig. 4. 3.and Fig. 4. 11. The average power density shows good linearity with the unit power level. Then the best-fitted linear function was used to read the power density in the experiment.

The volumetric power density was also verified by comparing it with the condensation heat removal rate of the steam produced. A stable steady-state operation of the boiling in the test section and condensation in the condenser of the loop was achieved. The reading of condensate liquid flow rate multiplied by the latent heat of vaporization is equal to the heat added in the test section to boil the liquid coolant. The comparison between the power input and latent heat of the condensate is shown in Fig. 4. 7 and Fig. 4. 13 and shows fairly a good agreement. The larger error at lower or higher power can be attributed to the rota-meter flow rate error caused by condensate temperature. The modified rota-meter scale was used the values of the condensate temperature 20, 40, 60 degrees (Table. 4. 1). It shows the level of enhancement of dryout heat flux in particle beds with the forced coolant flow from below.

Table 3. 1 Porosity of particle beds

	Dp = 4.8mm	Dp = 3.2mm
Porosity	0.38	0.37

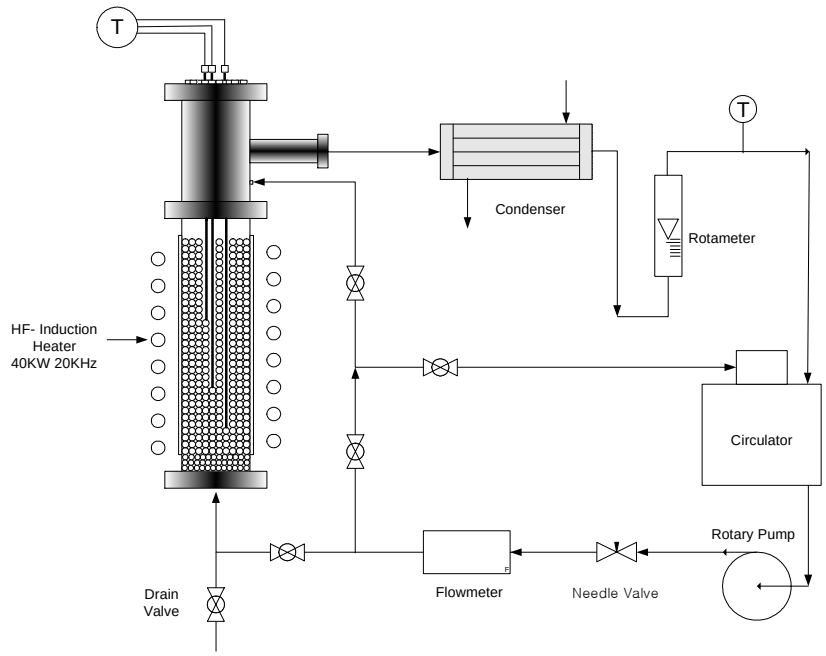

Figure 3 .1 Experimental setup

Figure 3. 2 H.F Induction Heater (Insung Co.)

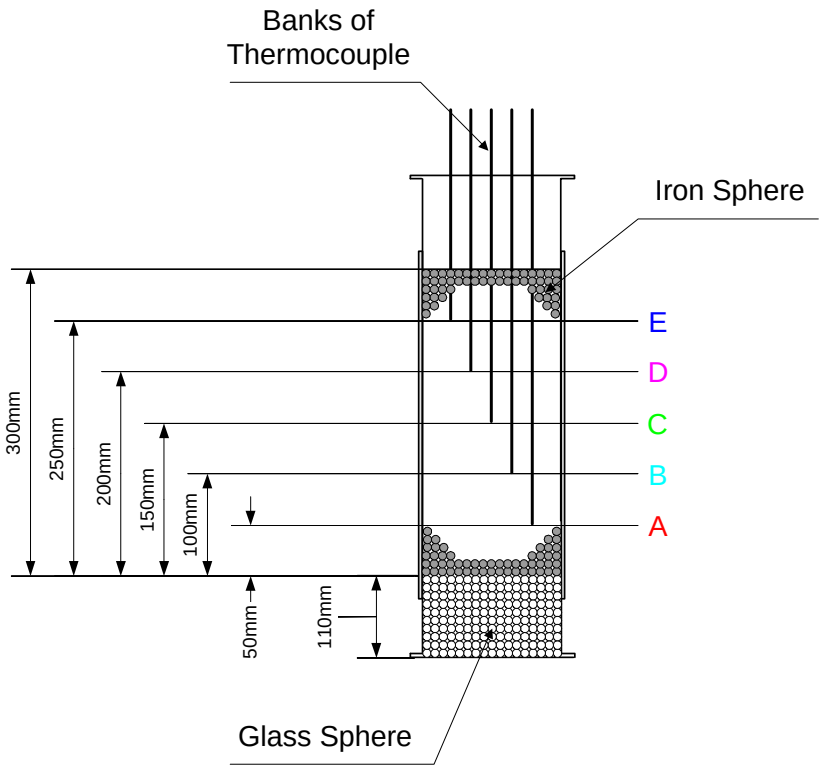

Figure 3. 3 Location of thermocouples

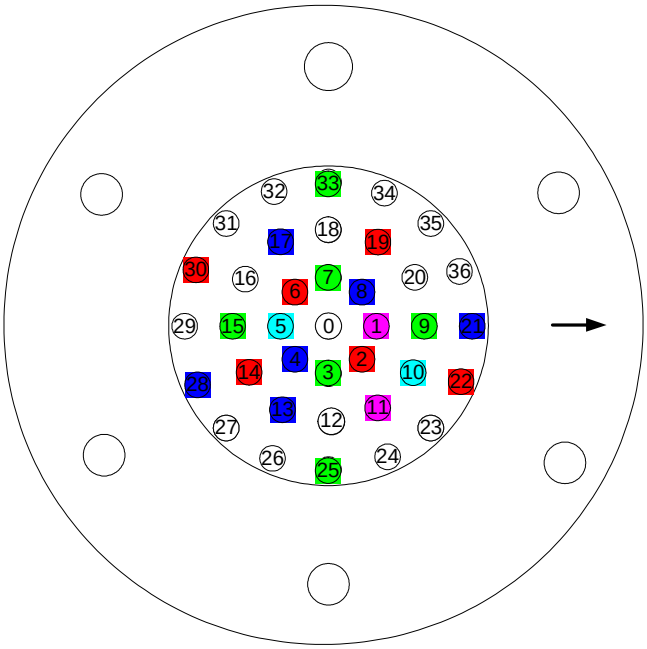

Location of Thermocouples in the Bank

A - 2, 6, 14, 19, 22, 30

B - 5, 10

C - 3, 7, 9, 15, 25, 33

D - 1, 11

E - 4, 8, 13, 17, 21, 28

0 is located on the bottom of Tube(0mm)

12 is located on the top of Tube (300mm)

Figure 3. 4 Radial distribution

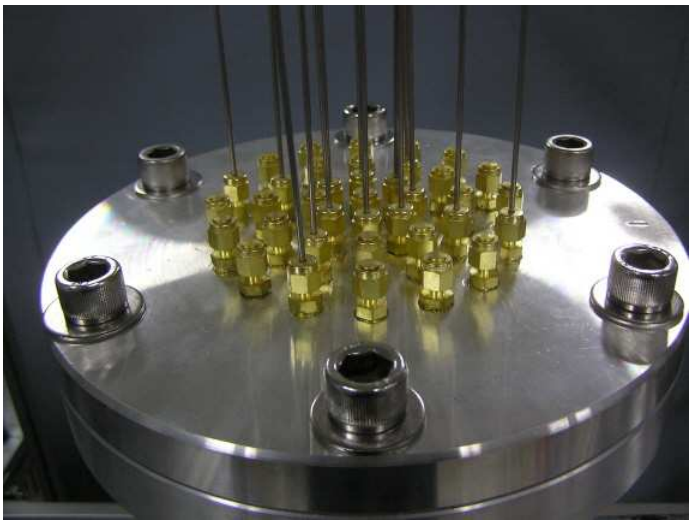

Figure 3. 5 Thermocouples on the top plate

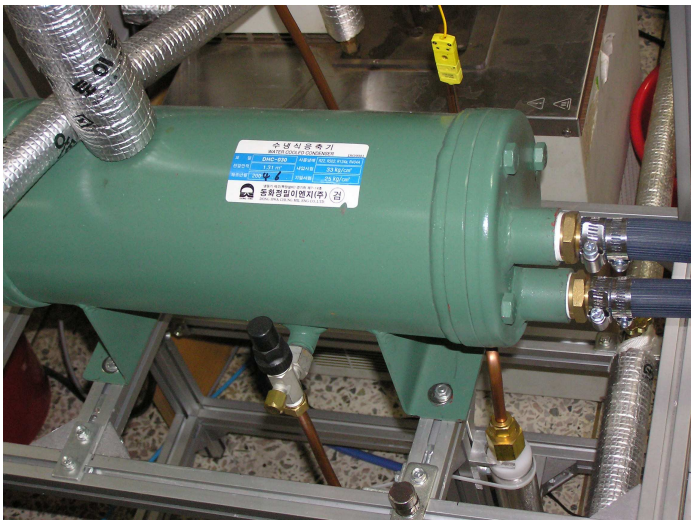

Figure 3. 6 Condenser (Dong Hwa Co.,DHC 030)

Figure 3. 7 Circulator (Fisher Co.)

Figure 3. 8 Coriolis-type mass flow meter (OVAL Co.)

Figure 3. 9 Condensate flowmeter (OMEGA Co.)

Figure 3. 10 Data Monitoring (Labview).

Figure 3. 11 Data acquisition system (NI Co.)

CHAPTER 4
EXPERIMENTAL RESULTS AND DISCUSSIONS

4.1 Test Condition

Experiment of dryout heat flux measurement for particle beds of 100 mm in diameter and 300 mm in height has been conducted. The water coolant is supplied either from the top of the bed or from below.

The bed is composed of steel particles in uniform size (4.8 mm diameter and 3.2mm diameter) and volumetrically heated by induction heater coil. In this experiment achievement of uniform heat input throughout the bed is crucial and for this purpose the particles composing the bed must be electrically isolated or completely conducted.

Complete conductance between the steel particles is not plausible in this case, however the natural rusting of steel particles after several repeated boiling had built sufficient oxide coating over the particle surface and this provided complete electrical insulation between the particles.

In order to measure the volumetric power density in the bed with induction heating, liquid coolant was filled up to the top of the bed and induction power was applied at a predetermined level. The liquid temperature was allowed to rise to the boiling temperature. The Calculation method of power density distribution is shown in Fig 4. 1.

The twenty-two thermocouple signals gave sensible heating of liquid and these values were converted to power density distribution. Natural circulation of the coolant in the bed caused nonlinear rise of temperature, particularly in the upper part of the bed (Fig. 4. 2). The banks of power density distribution are shown in Fig 4. 3. Although the center of the bed showed higher power and the top and the bottom parts of the bed were lower, the power density was uniform within 10%. The average power density at different power level of the induction unit is shown in Fig. 4. 4 and the average power density show good linearity with the unit power level. Then the best-fitted linear function was used to read the power density in the experiment.

The larger error at lower or higher power can be attributed to the rotameter flow rate error caused by condensate temperature. The rotameter flow scale modify to the proper temperature. The graph of modified flow scale is shown Fig 4. 5 and Fig 4. 6. Tables 4. 1 was shown in the modified rotameter scale as to the condensate temperature.

The volumetric power density was also verified by comparing it with the condensation heat removal rate of the steam produced. A stable steady-state operation of the boiling in the test section and condensation in the condenser of the loop was achieved. The reading of condensate liquid flow rate multiplied by the latent heat of vaporization is equal to the heat added in the test section to boil the liquid coolant. The comparison between the power input and latent heat of the condensate is shown in Fig. 4. 7 and shows fairly a good agreement.

4.2 The Effect of Dryout heat flux on the Bead Sizes

The first set of tests was top flooding case to obtain the top-flooding data for the present bed composition and geometry and also to verity the present experimental method by comparing with the past data of similar geometry. The nearly saturated liquid coolant is, in this case, continuously added to the top of bed and the induction heating power was increased by a step from a lower level until one of thermocouples showed a sharp increase. The typical thermocouple signals when dryout occurs are shown in Fig. 4. 7. In top-flooding cases the dryout occurred always at the bottom of the bed.

For 4.8 mm particle bed, the top-flooding dryout heat rate was ~4 MW/m^3 as shown in Fig. 4. 6 and this value falls within the range of the past experimental data (see Fig. 4. 9). The coolant-boiling rate corresponding to this amount of heat input is about 0.5 kg/m^2s in terms of mass flux. Therefore when the coolant is injected only from below of the bed, the dryout occurs whenever the power input is greater that the heat required to evaporate all the coolant injected from below.

In case of the tests of bottom injection, the nearly saturated liquid coolant is continuously injected from the bottom of the test section at a preset rate. The induction heating power was increased by a step from a lower level until one of thermocouples showed a sharp increase. It is noted that there is a layer of glass bead section of 110 mm height between the bottom of the test section and the steel bead particle bed to distribute the injected coolant over the cross section of the test section.

In the range of coolant injection rate of 0.5 ~ 1.5 kg/m^2s, the dryout heat rates were shown in Fig. 4. 8. Also is plotted a line of evaporation heat of complete vaporization of the coolant flow. The dryout heat rate increases as the coolant injection rate is increased; ~5.0 MW/m^3 at the coolant

mass flux of 0.5 kg/m^{2}s and 7.91 MW/m^3 at the coolant mass flux of 1.5 kg/m^{2}s in 4.8mm particle size.

In 3.2 mm particle size, the coolant injection rate ranges 1 kg/m^{2}s from 0.25 kg/m^{2}s. Also the dryout heat rate increases as the coolant injection rate is increased. The dryout heat rate is about 3MW/m^3 at the coolant mass flux of 0.25 m^{2}s and 6.3 MW/m^3 at the coolant mass flux of 1 kg/m^{2}s in 3.2mm particle size. The dryout heat rates were shown in Fig. 4. 14.

The present dryout data for 300 mm bed height and 4.8 mm mm particle diameter are compared with the past studies in Fig. 4. 9. The present data of dryout heat rate of zero flow case (top-flooding) agrees well with the past data. Comparing with KAERI data for coolant flow from below also shows the effect of bed height.

4.3 The Effect Dryout Heat Flux on the Mass Fluxes

Generally the dryout heat rate increases as the coolant injection rate is increased in the past study. In my case, experimental results are the same. In 4.8m particle size, the dryout heat rate is about 5 MW/m^3 at the coolant mass flux of 0.5 kg/m^2s and 7.91 MW/m^3 at the coolant mass flux of 1.5 kg/m^2s. The regime transition from flooding controlled dryout to bulk film boiling occurs at about 0.75 kg/m^2s (Fig. 4. 8).

In 3.2mm particle size, the dryout heat rate is about 3 MW/m^3 at the coolant mass flux of 0.25 kg/m^2s and 6.3 MW/m^3 at the coolant mass flux of 1 kg/m^2s (Fig 4. 9)

The comparisons of experimental results were shown in Fig. 4. 14 and Fig. 4. 15.

4. 4 The implications to the particle bed coolability

The test was conducted a top flooding case to obtain the dryout data and compared with the past data of similar geometry. The dryout occurred always at the bottom of the bed. Dryout occurs due to countercurrent flooding.

At the bottom injection case, Dryout areas are generally located in the upper part of the bed. The void fraction of the areas is high.The starting point of the dryout occurred both in the center as well as near the crucible wall.

In several cases, the coolant has temporarily not injected in particle beds. It was thought theat the pressure in the bed temporarily increased. Because the coolant was not injected from below. It was caused what not supplied the coolant in particle beds.

Table 4. 1 Conversion table for condensate flow rate with condensate temperature.

Scale	20 ℃ m	40 ℃ m	60 ℃ m	m_{40} / m_{20}	m_{60} / m_{20}
10	0.055	0.073	0.0895	1.3273	1.6273
15	0.106	0.121	0.139	1.1415	1.3113
20	0.15	0.174	0.189	1.1600	1.26
25	0.201	0.223	0.24	1.1094	1.1940
30	0.252	0.275	0.292	1.0913	1.1587
40	0.351	0.38	0.397	1.0826	1.1310
50	0.445	0.47	0.487	1.0562	1.0944
60	0.539	0.587	0.615	1.0890	1.1410
90	0.88	0.926	0.96	1.0523	1.0909

Table 4. 2 Measured dryout heat rate (Dp=4.675mm)

TEST (No)	Mass Flux (kg/m^2s)	Power Level (%)	Vol. Power Input (MW/m3)	Time to dryout (min)
1	0	26	4.221	6
2	0	24	3.896	29
3	0	24	3.896	21
4	1	42.5	6.819	2
5	1	40	6.494	19
6	1	37.5	6.105	9
7	1	42.5	6.819	14
8	1.25	50	7.710	15
9	1.5	57	7.910	18
10	0.75	39	6.332	8
11	0.75	39	6.332	11
12	0.5	30	4.871	5
13	0.5	27	4.383	21

Table 4. 3 Measured dryout heat rate (Dp=3.175mm)

TEST (No)	Mass Flux (kg/m^2s)	Power Level (%)	Vol. Power Input (MW/m3)	Time to dryout (min)
1	0	20	3.13	6
2	0	17.5	2.74	7
3	0	17.5	2.74	4
4	1	32.5	5.07	13
5	0.5	27.5	4.29	2
6	0.25	17.5	2.74	10
7	0.75	35	5.46	15
8	1	40	6.24	14
9	0.25	19	2.97	1
10	0.5	28	4.37	9
11	0.75	35	5.46	4

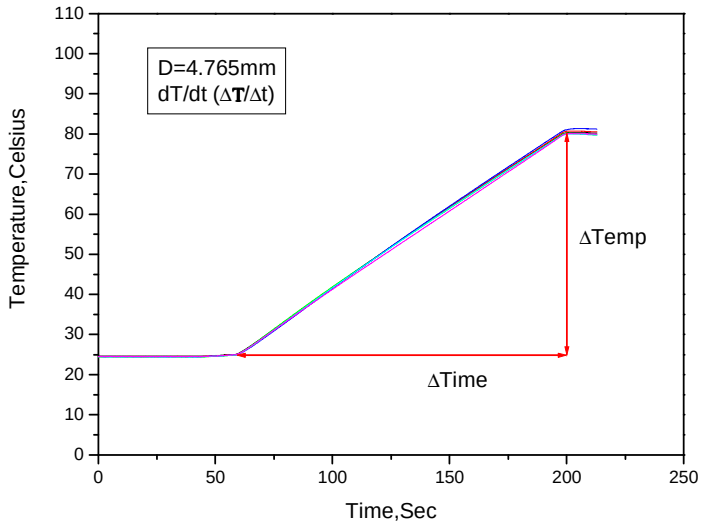

Figure 4. 1 Bed heatup rate

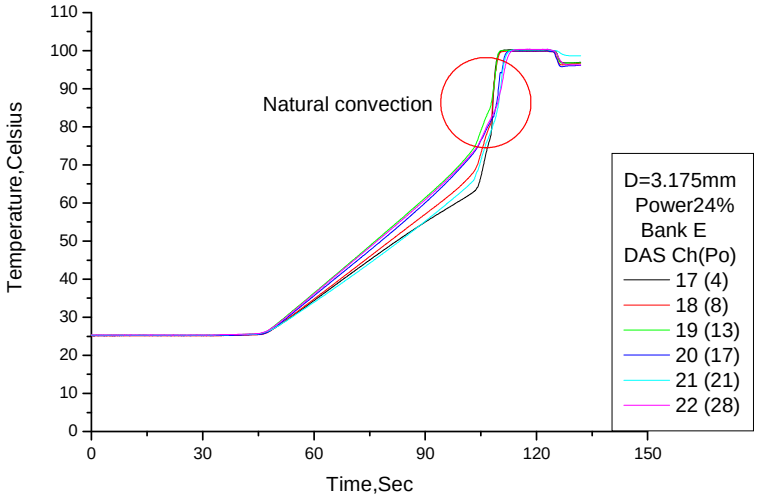

Figure 4. 2 The Natural convection

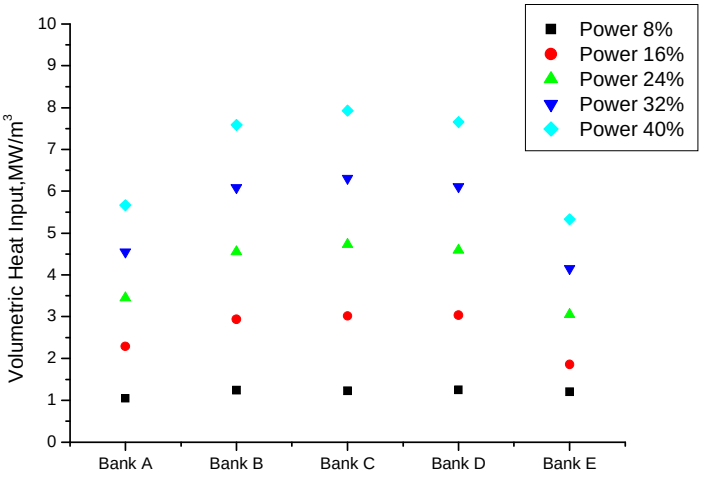

Figure 4. 3 Power densities at each bank (D=4.8mm)

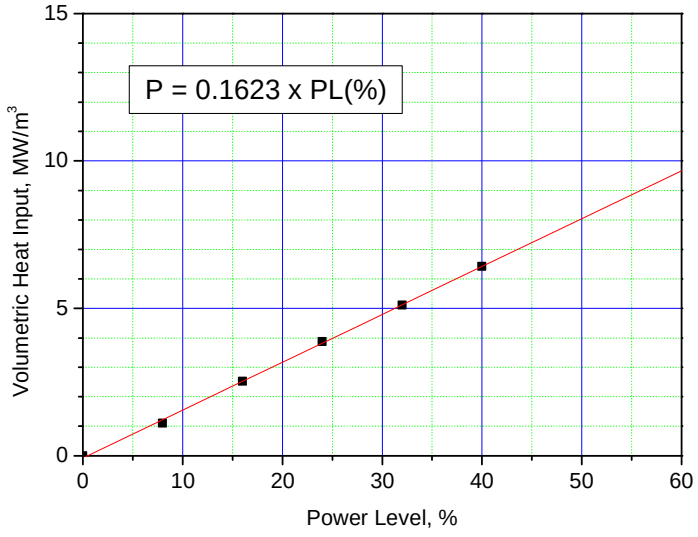

Fig. 4. 4 Volumetric power densities (Dp=4.8mm)

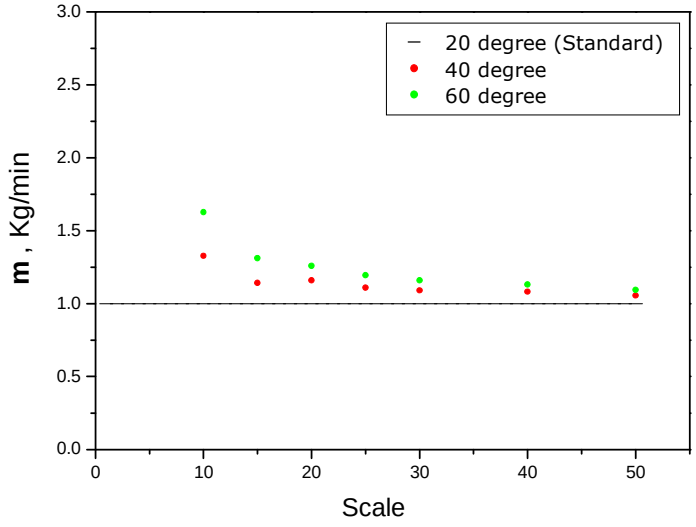

Fig. 4. 5 The modified flow scale in terms of the condenser temperature A.

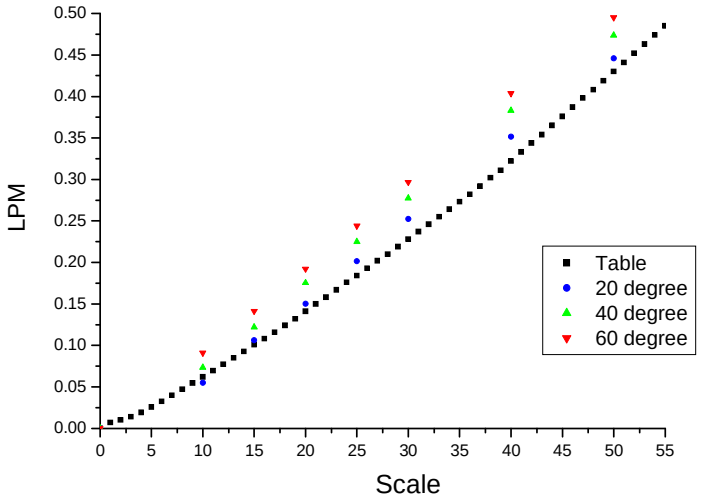

Fig. 4. 6 The modified flow scale in terms of the condenser temperature B.

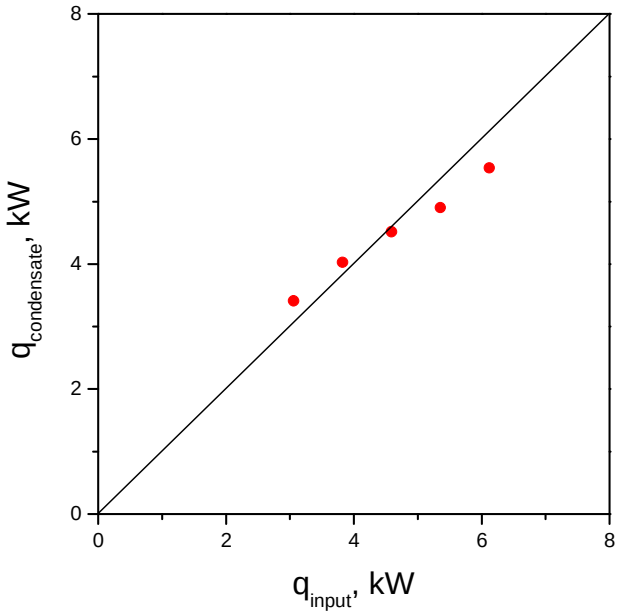

Fig. 4. 7 Comparison of energy balance (Dp=4.8mm)

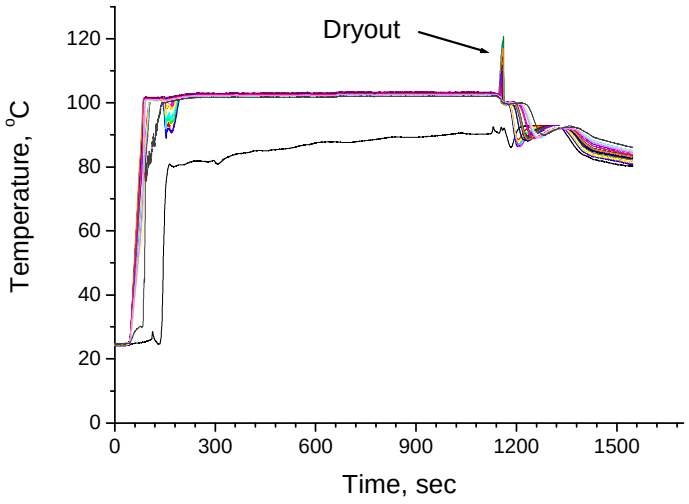

Fig. 4. 8 Typical temperature responses at dryout

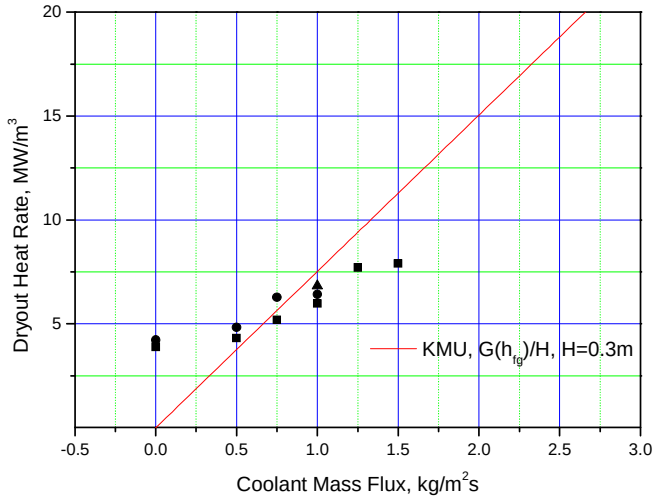

Fig. 4. 9 Experimental results of dryout heat rate

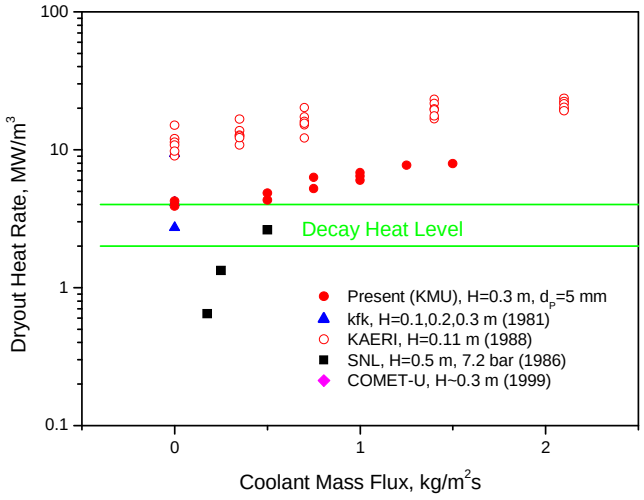

Fig. 4. 10 Comparison of experimental results (Dp=4.8mm)

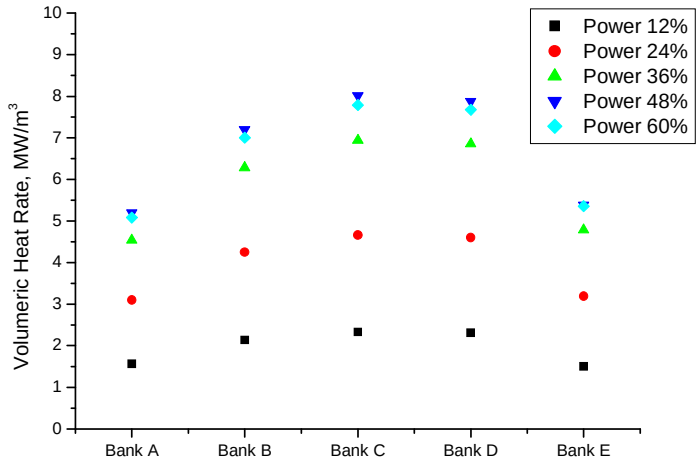

Figure 4. 11 Power densities at each bank (D=3.2mm)

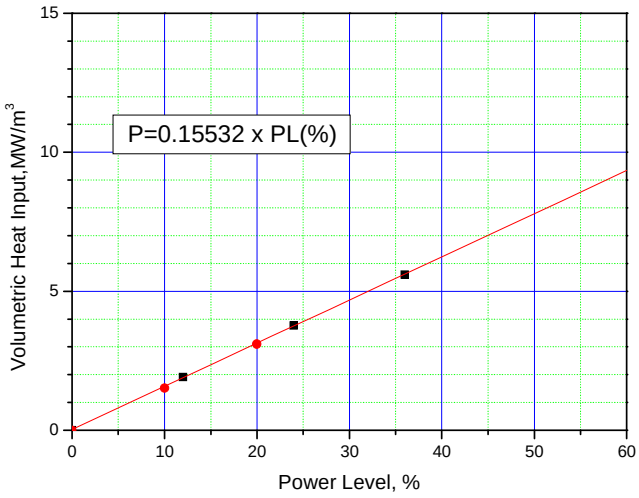

Fig. 4. 12 Volumetric power densities (Dp=3.2mm)

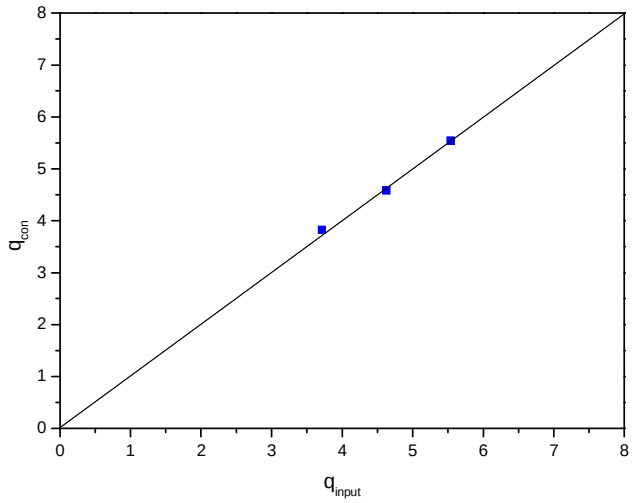

Fig. 4. 13 Comparison of energy balance (Dp=3.2mm)

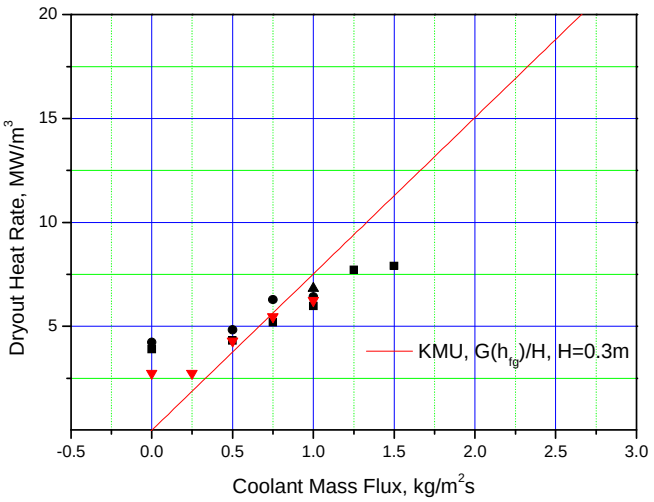

Fig. 4. 14 Experimental results of dryout heat rate
(Dp=4.8mm and Dp=3.2mm)

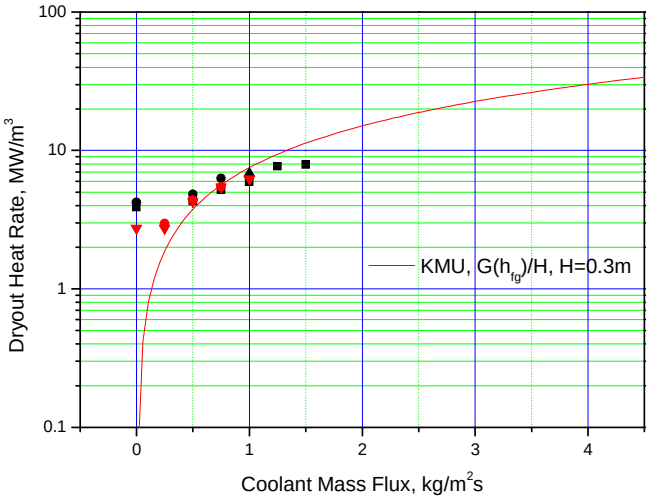

Fig. 4. 15 Comparison of experimental results

(Dp=4.8mm and Dp=3.2mm)

CHAPTER 5

CONCLUING REMARKS

Enhancement of dryout heat flux in debris beds with coolant flow from below has been experimentally studied. A fairly uniform heating of particle bed was achieved by induction heating.

The dryout heat rate data were obtained for both top-flooding case and forced coolant injection from below with the injection mass flux up to 1.5 kg/m^2s. For the top-flooding case, the volumetric dryout heat rate was about 4 MW/m^3 in 4.8 mm particle and about 3 MW/m^3 in 3.2mm particle. At the coolant injection mass flux of 1.5 kg/m^2s, the volumetric dryout heat rate was about 7.91 MW/m^3 in 4.8mm particle. In 3.2mm particle, at the coolant injection mass flux of 1 kg/m^2s, the volumetric dryout heat rate was about 6.3 Mw/m^3. It shows the level of enhancement of dryout heat flux in particle beds with the forced coolant flow from below.

The dependence of dryout heat rate on particle diameter will be further investigated by conducting the tests with smaller particle diameters. Also an analytical model of dryout heat rate will be developed by accounting for the effect of upward coolant flow in Particle beds.

REFERENCE

Alsmeyer, H. and Tromm, W. (1999), “The COMET Concept for Cooling Core Melts: Evaluation of the Experimental Studies and Use in the EPR,” FZKA 6186, EXV-CSC (99)-D036.

Atkhen, K. and Berthoud, G. (2003), “Experimental and Numerical Investigations on Debris Bed Coolability in a Multidimensional and Homogeneous Configuration with Volumetric Heat Source,” Nuclear Technology, 142, pp. 270-282.

Barleon, L. et al. (1984), “Cooling of Debris Beds,” Nuclear Technology, 65, pp. 67-86.

Buchlin, J.M. et al. (1989), “Thermohydraulics of Heated Porous Media Associated with Nuclear Reactor Safety,” Transport Process in Porous Media, U.S.A., pp. 315-370

Cha, J.H. et al. (1986), “Degraded Core Cooling,” J. Korean Nuclear Society, 18(1), pp.48-70.

Cha, J. H. et al. (1986), “Forced Flow Dryout Heat Flux in Heat Generating Debris Bed,” J. Korean Nuclear Society, 18(4), pp. 273-280.

Farmer, M. T. et al. (1992), “Results of MACE Test M0 and M1,” Proceedings of the 2nd OECD (NEA) CSNI Specialist's

Meeting on Molten Core Debris-Concrete Interactions, Karlsruhe, Germany.

Hohmann. H. et al. (1997), “FCI Experiments in Corium/Water System,” Nucl. Eng. Des., 177, p. 339-349.

Hu, K. and Theofanous, T. G. (1991), “On the Measurement and Mechanism of Dryout in Volumetrically Heated Coarse Particle Beds,” Int. J. Multiphase Flow, 17(4), pp. 519-532.

Kazachkov I. V. and Konovalikhin M. J. (2002), “Steam flow through the volumetrically heated particle bed,” Int. J. Thermal Sciences, 41, pp. 1077-1087.

Kim, S. H. (1996), “A Modeling of the Liquid-Vapor Flow in a Self-Heated Porous Medium: With Application to the Dryout Limits,” J. Nuclear Science and Technology, 33(9), pp. 686-695.

Klockow, H. B. et al. (2003), “Simulant Melt Pool Quench Behavior via Coolant Injection from Below,” Proc. 10th Int. Topical Meeting on Nuclear Reactor Thermal Hydraulics (NURETH-10), Seoul.

Lipinski, R. J. (1984), “A Coolability Model for Postaccident Nuclear Reactor Debris,” Nuclear Technology, 65, p. 53.

Naik, A.S. and Dhir, V.K., ”Forced Flow Evaporative Cooling of a Volumetrically Heated Porous Layer,” Int. J. Heat Mass Transfer, vol.25,

pp.541-552, 1982

Tsai, F. P. and Catton, I. (1983), “On Dryout Heat Flux and Pressure Drop of a Submerged Inductively Heated Bed Flow From Below,” Proc. Nat. Heat Transfer Conf., AIChe Symposium Series, 79(225), pp. 296-302.

Turland, B. D. and Moore, K. (1983), “Debris Bed Heat Transfer with Top and Bottom Cooling,” Proc. Nat. Heat Transfer Conf., AIChe Symposium Series, 79(225), pp. 250-255.

SUMMARY IN KOREAN

본 논문은 냉각수 하단 주입시 파편 층에서의 Dryout Heat Flux 에 미치는 영향을 고찰하기 위해 실험적 연구로 수행되었다.

실험장치의 주요 구성으로는 유도가열기(40kW, 30kHz), 높이 300 mm, 내부 지름이 100 m 인 이중벽 Quartz Tube 그리고 콘덴서로 폐회로(Recovery condenser loop)를 구성하였다. 쇠구슬의 크기는 모두 같으며, 4.8 mm 와 3.2 mm 를 사용하였다.

상부 주입의 경우(Top-flooding case)에 4.8 mm 크기에서 Dryout Heat Flux은 약 4 MW/m^3 이고3.2 mm에서는 Dryout Heat Flux는 약 3 MW/m^3 이다.

하단 주입시(Bottom Injection case) 4.8 mm 크기에서 냉각수가 1.5 kg/m^2s일 때 Dryout Heat Flux은 약 7.9 MW/m^3 이고, 3.2mm 크기에서는 냉각수가 1.0 kg/m^2s일 때 약 6.3 MW/m^3 이다. 냉각수량이 증가할수록 Dryout Heat Flux가 증가하는 경향을 나타내었다.

ACKNOWLEDGEMENT

지금은 배우는 시기라고.... 스스로 부족함을 채우기 위해 여기까지 왔습니다. 그리고 벌써 대학원 생활도 끝나 가고 있습니다. 되돌아보면 어렵고 힘들기도 했지만 이 모든 것들이 아쉬움과 감사함으로 다가옵니다. 또다시 부족함을 메우기 위해 시작하려 합니다. 어느 곳에서든 사랑을 나누어 주며 한 걸음씩 나아가렵니다.

삶에서도, 지식에서도 스승이신 방광현 지도교수님께 먼저 감사 드립니다. 부족한 제자를 참아주시고 가르쳐 주시느라 고생하신 교수님... 감사합니다. 오랜 기간 동안 많은 가르침을 주신 김동혁 교수님, 삶이 감동이신 도덕희 교수님, 윤상국 교수님, 정형호 교수님께도 감사드립니다. 먼저 실험실을 나간 재경선배, 선식이형, 경수선배, 영아와 대학원 생활에서 동고동락한 태영선배, 동기 원호, 동생 종욱, 양호, 실험을 도와주느라 고생 많이 한 아들 군의, 옥근, 경규에게 고마움을 전합니다. 정혜선배와 나의 동기들 동진, 구만, 경록, 윤석 그리고 창렬씨에게도 고마움을 전합니다.

무엇보다 아들을 믿으시며 지켜봐 주신 부모님께 감사 드립니다. 아들을 위해서 밤낮으로 고생하시며 뒷바라지 하신 부모님의 그 사랑을 늘 기억하며 살겠습니다. 나의 사랑하는 동생들 현정, 건우에게도 고마움을 전합니다. 언제나 곁에 있어주며 용기를 북돋아 준 사랑하는 현아에게 고마움을 전합니다. 죽마고우 친구들 과 블리스-엘리웃-한니엘 친구들에게도 고마움을 전합니다.

사랑합니다.

내 삶의 목적과 방향되신 하나님께 모든 영광을 드립니다.